Multi-Context Fusion Transformer for Pedestrian Crossing Intention Prediction in Urban Environments

Yuanzhe Li 1*, Hang Zhong 1, Steffen Müller 1

¹Chair of Automotive Engineering, Technische Universität Berlin, Berlin, 13355, Germany *yuanzhe.li@campus.tu-berlin.de

Abstract: Pedestrian crossing intention prediction is essential for autonomous vehicles to improve pedestrian safety and reduce traffic accidents. However, accurate pedestrian intention prediction in urban environments remains challenging due to the multitude of factors affecting pedestrian behavior. In this paper, we propose a multi-context fusion Transformer (MFT) that leverages diverse numerical contextual attributes across four key dimensions, encompassing pedestrian behavior context, environmental context, pedestrian localization context and vehicle motion context, to enable accurate pedestrian intention prediction. MFT employs a progressive fusion strategy, where mutual intra-context attention enables reciprocal interactions within each context, thereby facilitating feature sequence fusion and yielding a context token as a context-specific representation. This is followed by mutual cross-context attention, which integrates features across contexts with a global CLS token serving as a compact multi-context representation. Finally, guided intra-context attention refines context tokens within each context through directed interactions, while guided cross-context attention strengthens the global CLS token to promote multi-context fusion via guided information propagation, yielding deeper and more efficient integration. Experimental results validate the superiority of MFT over state-of-the-art methods, achieving accuracy rates of 73%, 93%, and 90% on the JAAD_{beh}, JAAD_{all}, and PIE datasets, respectively. Extensive ablation studies are further conducted to investigate the effectiveness of the network architecture and contribution of different input context. Our code is open-source: https://github.com/ZhongHang0307/Multi-Context-Fusion-Transformer.

1. Introduction

With the rapid advancements in artificial intelligence and sensor technologies in recent years, autonomous vehicles (AVs) have been increasingly deployed in urban environments. The rapid deployment of AVs has raised significant safety concerns for vulnerable road users (VRUs), particularly pedestrians, due to the increasing frequency of pedestrian-AV interactions. Ensuring pedestrian safety requires AVs to have the ability to anticipate pedestrian intentions. Accurate pedestrian crossing intention prediction supplies critical contextual cues, enabling AVs to make safe decisions and exercise reliable control [1]. However, predicting pedestrian intentions in urban environments remains challenging, given the variability of pedestrian behavior and the complex influence of multiple environmental factors, such as vehicle states and traffic conditions.

Predicting pedestrian crossing intention has attracted considerable research interest, with numerous studies employing vehicle-mounted camera footage. Representative datasets such as JAAD [2] and PIE [3] provide publicly accessible video data for analyzing pedestrian behavior in urban environments. Initial research efforts primarily relied on unimodal inputs, where researchers attempted to extract visual appearance features from images [2], spatial position features from pedestrian bounding boxes [8], or kinematic features from body pose data [9] for pedestrian intention prediction. For instance, Fang et al. employed convolutional neural network (CNN)-based pose estimation to extract pedestrian skeletons, and stacked multi-frame skeleton sequences as input to support vector machine or random forest classifiers for intention prediction [9]. However, such methods show poor performance in complex traffic conditions, where multiple contextual factors affect pedestrian crossing decisions. For instance, relying solely on pedestrian skeletons information fails to capture critical contextual cues, such as the presence of zebra crossings or vehicle motion trends, both of which can significantly influence a pedestrian's decision to cross

Recent studies have integrated diverse modalities to capture both pedestrian-specific behaviors and broader environmental dynamics. Specifically, subsequent works have employed visual modalities such as semantic maps that encode scene semantics [4] and optical flow that characterizes motion patterns [10], as well as non-visual modalities including vehicle speed reflecting dynamic states [6] and bounding box coordinates indicating pedestrian locations [5], to enhance the accuracy of pedestrian intention prediction. Building upon these advances, various multimodal feature fusion methods have been proposed to effectively combine heterogeneous modalities, aiming to exploit their complementary strengths and further improve prediction performance. In [11], WatchPed is proposed, where non-visual inputs (vehicle speed, bounding box, pose keypoints) are processed through stacked gated recurrent unit (GRU), visual inputs (pedestrian local patches and global images) are extracted via a hybrid convolutional neural network (CNN)-GRU framework, and after initial fusion with attention weights, the combined features are integrated with pedestrian motion data from the smartwatch sensor branch for intention prediction. Global PCPA [4] employs a CNN-GRU pipeline for visual feature extraction and utilizes GRU encoders for non-visual modalities. This architecture adopts a hierarchical attention mechanism, first applying temporal attention to weight contributions across continuous frames, followed by modality attention to learn fusion weights for each modality.

Although most prior studies rely on directly modeling high-dimensional raw modality data such as RGB images in an end-to-end manner, this strategy has several inherent limitations. First, due to the high dimensionality and redundancy of raw data, such modeling is computationally intensive and often yields over-parameterized models prone to overfitting on the training scenarios, thus reducing flexibility and limiting generalization across diverse traffic environments. Moreover, features derived from raw modalities are typically implicit and entangled. In addition, they tend to be sensitive to noise, lack explicit semantic representations, and require substantial amounts of data, all of which collectively hinder training efficiency. In this work, we employ numerical contextual attributes derived from raw sensor data, which abstract low-level observations into compact and explicitly semantic representations spanning four critical dimensions: pedestrian behaviors, environmental conditions, pedestrian localization, and vehicle motion dynamics. The complementarity among these dimensions facilitates a more comprehensive characterization of pedestrian crossing intentions, thereby offering a lightweight and efficient alternative to raw modality-based approaches.

The main contributions are summarized as follows: (1) We propose a multi-context fusion Transformer (MFT) that leverages diverse numerical contextual attributes with complementary characteristics, encompassing both discrete and continuous forms from four critical dimensions, namely behavior context, environmental pedestrian localization context and vehicle motion context, to predict the crossing intention of the target pedestrian. (2) A progressive fusion strategy is designed to sequentially process multi-context data, beginning with intra- and cross-context fusion through reciprocal interactions, followed by intra- and cross-context refinements via directed interactions, with taskspecific attention mechanisms guiding each stage. (3) Extensive experiments and ablation studies on the JAAD and PIE datasets are conducted to validate the performance of the proposed MFT network and the rationality of its network architecture.

2. Related works

Pedestrian crossing intention prediction has attracted extensive research attention, and many works rely on vehiclemounted video recordings to investigate pedestrian behaviors. Public datasets such as JAAD [2] and PIE [3] offer annotated video sequences collected in urban traffic, serving as standard benchmarks for evaluating pedestrian intention prediction methods. Early works mainly utilized unimodal inputs, e.g., RGB image [2], pedestrian bounding box [8], or body pose information [9], for pedestrian intention prediction. In [2], the authors investigated the prediction of pedestrian intentions based on static images capturing either the lower or the upper body. In [7], pedestrian position coordinates are extracted via stereo vision using median disparity computation from bounding box regions, which are subsequently processed by a stacked long short-term memory (LSTM) architecture to capture temporal dependencies for intention prediction. However, these methods often perform poorly in complex traffic scenarios, where pedestrian crossing decisions are influenced by multiple contextual factors. For instance, approaches that rely solely on pedestrian images tend to neglect essential environmental cues, such as crosswalk

availability and surrounding vehicle dynamics, which play an essential role in shaping pedestrian behavior.

In subsequent studies, a variety of multimodal fusion methods have been introduced to better understand pedestrian behavior by leveraging complementary information from multiple modalities. Different visual inputs (such as semantic maps in [4], and optical flow in [10]) and non-visual inputs (such as bounding box coordinates in [5] and vehicle speed in [6]) have been integrated to capture both pedestrian-specific behaviors and broader environmental dynamics. SF-GRU, introduced in [17], employs a stacked RNN framework to gradually combine five different modalities, including pedestrian appearance, environmental context, body pose keypoints, bounding box information, and vehicle speed, through hidden state stacking. In [4], Global PCPA framework integrates a CNN-GRU pipeline for visual processing with GRU-based encoders for non-visual data. Its hierarchical attention mechanism sequentially applies temporal weighting across frames and modality weighting across different feature sources. The V-PedCross framework [8] adopts a virtual-toreal distillation strategy, passing rich multimodal knowledge (e.g., optical flow) from a synthetic-data teacher network to a compact student model, thereby balancing efficiency and predictive accuracy.

Given the significant success of Transformers in sequential modeling and computer vision applications, researchers have increasingly adopted Transformer-based architectures for multimodal feature fusion. Transformers have been applied to distinct feature extraction tasks, covering modalities from visual to non-visual. For instance, CAPformer [31] employs a Transformer to extract features from stacked non-visual modalities, including bounding boxes, pose keypoints, and vehicle speed, which are then fused with visual features obtained by RubiksNet for intention prediction. Similarly, Action-ViT [30] arranges visual modalities along the temporal dimension and converts non-visual inputs into pseudo-images, which are processed by a pre-trained Vision Transformer for temporal representation learning, followed by modality-level attention. TAMformer [14] employs independent Transformer blocks to encode bounding boxes, pose keypoints, and local context images, and introduces learned attention masks for adaptive temporal modeling. In addition to feature extraction, Transformers have also been utilized to fuse multimodal features, enabling the integration of heterogeneous information sources. In [12], PIT is proposed, where an interaction Transformer layer is designed to model interactions between tokenized global RGB images, pedestrian pose data, and vehicle speed within each frame, followed by a temporal fusion block for temporal integration. PedCMT [13] employs a cross-modal self-attention mechanism to fuse pedestrian bounding box features with vehicle speed, capturing their complementary relationships for intention prediction.

Most existing studies model high-dimensional raw modalities (e.g., RGB images) in an end-to-end manner, which is computationally expensive and tends to yield over-parameterized models that overfit training data, thereby limiting flexibility and generalization in diverse traffic environments. Moreover, the features derived from raw data are typically implicit and entangled, leading to low efficiency in representation learning. In contrast, our work explores an alternative approach by leveraging numerical contextual attributes derived from raw sensor data and enriched with

explicit semantics, providing compact representations across multiple dimensions such as pedestrian behaviors, environmental conditions, pedestrian localization, and vehicle motion dynamics.

3. Methodology

3.1 Problem Formulation

The prediction task is formulated as a binary classification problem, defined as follows: given a fixed-length video sequence captured by an onboard camera and the egovehicle's motion data, the objective is to predict whether the target pedestrian j will exhibit crossing behavior $a_j \in \{0, 1\}$ at a specific future time instant. The observation window spans 0.5 seconds, comprising N consecutive frames (N=16) from a 30 FPS video sequence, with the final observation frame occurring at time t. The prediction horizon τ extends from the last observation frame t to the decision event, corresponding to the time-to-event (TTE), and ranges between 1-2 seconds (30-60 frames). The terminal frame is positioned immediately prior to the decision event, specifically defined as either the crossing initiation frame in crossing cases or the last observable frame in non-crossing cases.

3.2 Input Representation

The MFT network integrates four types of per-frame context, which provide complementary characteristics related to pedestrians, vehicles, and traffic environment, as illustrated in Fig. 1. These contexts are described as follows:

- 1. Pedestrian behavior context P: This context employs discrete numerical attributes to depict pedestrian's non-verbal behavioral characteristics. It provides informative cues about pedestrian behavioral states and interaction patterns. P encompasses several behavioral categories: motion state (standing or walking), gaze state (looking or not looking), head nod (nodding or others), hand gesture (greeting, yielding, right-of-way, or others), and motion direction (lateral, longitudinal, or others). For the PIE dataset, the head nod category is incorporated into the hand gesture category. Therefore, P has a shape of $N \times 5$ for JAAD dataset and $N \times 4$ for PIE dataset.
- 2. Pedestrian localization context *L*: This context describes the pedestrian's spatial position within the image. It is represented by the bounding box coordinates (top-left and

bottom-right corners) and has a shape of $N\times4$. It provides critical insights into pedestrian movement dynamics and spatial behavior patterns that provide early indicators of crossing decisions.

- 3. Vehicle motion context V: This context represents the ego-vehicle's kinematic state, modeled through velocity profiles derived from dataset annotations, with a shape of $N \times 1$. It serves as a key predictor in pedestrian intention modeling, for instance, deceleration patterns signal driver yielding behavior, which pedestrians may interpret as crossing opportunities.
- 4. Environmental context E: This context utilizes discrete numerical attributes to represent the traffic environment infrastructure. It provides essential information about the road layout, traffic signage, and static environmental elements that influence pedestrian-vehicle interactions. E encompasses several environmental categories: number of lanes, intersection existence, crosswalk availability, traffic light status (red, green, or others), traffic direction (one-way or two-way), road type (street, parking lot, or garage), stop sign presence, and signage type. In the PIE dataset, the road type and stop sign presence attributes are not provided, but stop sign presence can be inferred from the signage type category. Therefore, E has a shape of $N \times 8$ for JAAD dataset and $N \times 7$ for PIE dataset.

To represent these contexts in a unified form, the discrete attributes are encoded using label encoding, while the continuous attributes are preserved in their original numerical form. The multi-context fusion Transformer (MFT) adopts a progressive fusion strategy that hierarchically integrates intra-context features and fuses complementary multi-context information for pedestrian intention prediction. The overall architecture of MFT is illustrated in Fig. 2, and detailed descriptions of its key modules are provided in the subsequent sections.

3.3 Intra-Context Fusion

The intra-context fusion (ICF) module captures temporal dependencies and performs an early-stage fusion of features within each context, generating modality-specific feature sequences with fused temporal information. Specifically, for context i ($i \in \{P, L, V, E\}$), the raw inputs are first projected

to a high-dimensional feature sequence $F_i \in \mathbb{R}^{N \times 128}$ through

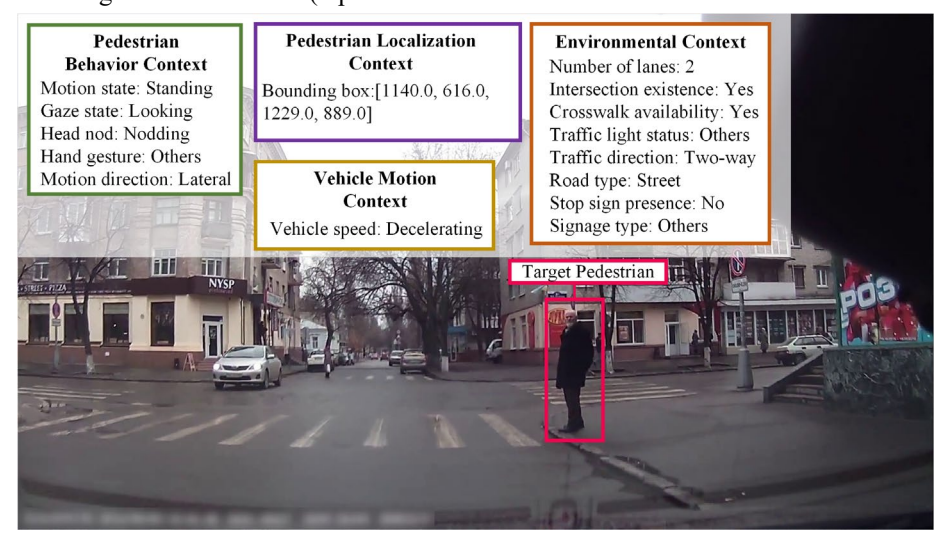


Fig. 1 Illustration of multi-context annotations in a traffic scene

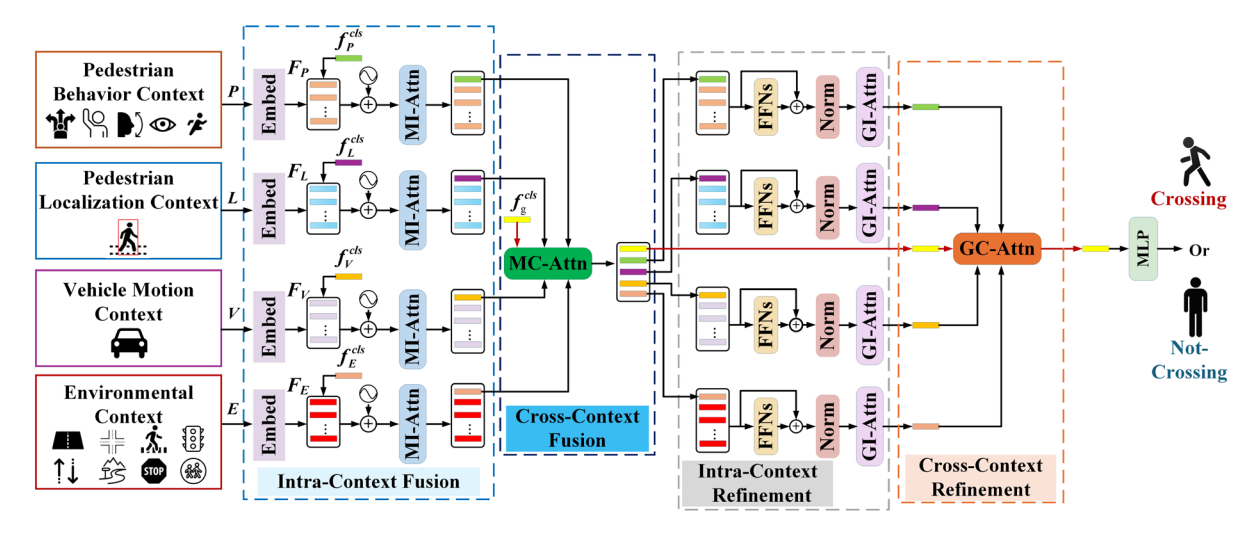


Fig. 2 The architecture of the proposed MFT network

embedding layers. A learnable context token f_i^{cls} is prepended to the feature sequence F_i along the temporal axis, serving as a compact context-specific representation. Sinusoidal positional encodings (PE) are added to maintain temporal order information, producing the position-encoded feature sequence $F_i' \in \mathbb{R}^{(N+1) \times 128}$:

$$F_{i}' = \left[f_{i}^{cls}, f_{i}^{t-N+1}, ..., f_{i}^{t} \right] + PE$$
 (1)

Where PE is defined as:

$$\begin{cases}
PE(pos, 2k) = \sin\left(\frac{pos}{10000^{\frac{2k}{d}}}\right) \\
PE(pos, 2k+1) = \cos\left(\frac{pos}{10000^{\frac{2k}{d}}}\right)
\end{cases}$$
(2)

To model global temporal correlations within individual contexts, we introduce a mutual intra-context attention (MI-Attn) mechanism that explicitly facilitates reciprocal interactions among the feature sequence. MI-Attn comprises multi parallel attention heads that simultaneously capture information across multiple representation subspaces. For attention head n, the temporal attention is calculated as:

$$\alpha_{i,n}^{\text{MI-Attn}} = \text{Softmax}\left(\frac{Q'_{i,n} \cdot K'_{i,n}^T}{\sqrt{d}}\right)$$
 (3)

Where $Q'_{i,n} = F'_i \cdot W^{\mathcal{Q}}_{i,n}$ and $K'_{i,n} = F'_i \cdot W^{\mathcal{K}}_{i,n}$ are query and key of context i. And $\alpha^{\text{MI-Attn}}_{i,n} \in \mathbb{R}^{(N+1)\times (N+1)}$ represents the temporal attention matrix encoding pairwise attention weights across the sequence.

By multiplying $V'_{i,n}$ with $\alpha^{\text{MI-Attn}}_{i,n}$, the context token fuse temporal information across the entire sequence, with individual frame features simultaneously being enriched:

$$\tilde{F}_{i,n} = \alpha_{i,n}^{\text{MI-Attn}} \cdot V_{i,n}' \tag{4}$$

Where $V'_{i,n} = F'_i \cdot W^V_{i,n}$ is the value of context *i*.

The outputs from all attention heads are concatenated and linearly projected to obtain the final ICF module output $\tilde{F}_i = [\tilde{f}_i^{cls}, \tilde{f}_i^{t-N+1}, ..., \tilde{f}_i^t]$.

3.4 Cross-Context Fusion

The cross-context fusion (CCF) module enables feature interaction across contexts, performing an early-stage multicontext fusion and facilitating complementary information exchange. Specifically, all updated context tokens from the ICF module are extracted and combined with a learnable global CLS token $f_{\rm g}^{cls}$, which serves as a compact global context representation. The context tokens $F_C = \left[f_{\rm g}^{cls}, \tilde{f}_P^{cls}, \tilde{f}_L^{cls}, \tilde{f}_V^{cls}, \tilde{f}_E^{cls}\right] \text{ are then fed to the mutual cross-context attention (MC-Attn) mechanism, which is designed to model inter-context correlations. MC-Attn employs multi attention heads for parallel multi-subspace modeling. For attention head <math>m$, the cross-context attention is computed as:

$$\alpha_m^{\text{MC-Attn}} = \text{Softmax}\left(\frac{\tilde{Q}_m \cdot \tilde{K}_m^T}{\sqrt{d}}\right)$$
 (5)

Where \tilde{Q}_m and \tilde{K}_m are query and key matrices obtained by applying learnable projections \tilde{W}_m^Q and \tilde{W}_m^K to F_C . $\alpha_m^{\text{MC-Attn}} \in \mathbb{R}^{5\times 5}$ denotes the cross-context attention matrix that encodes pairwise attention weights between different contexts

By multiplying \tilde{V}_m with $\alpha_m^{\text{MC-Attn}}$, the global CLS token integrates information from context-specific representations, enabling early-stage multi-context fusion, while the individual context tokens simultaneously exchange and incorporate information from other contexts:

$$\tilde{F}'_{C,m} = \alpha_m^{\text{MC-Attn}} \cdot \tilde{V}_m \tag{6}$$

Where \tilde{V}_m is the value matric obtained by applying learnable projections \tilde{W}_m^V to F_C .

The outputs from all attention heads are then concatenated and linearly projected to obtain the final CCF module output $\tilde{F}_C' = \left\lceil \tilde{f}_g^{\prime cls}, \tilde{f}_P^{\prime cls}, \tilde{f}_L^{\prime cls}, \tilde{f}_V^{\prime cls}, \tilde{f}_E^{\prime cls} \right\rceil$.

3.5 Intra-Context Refinement

The intra-context refinement (ICR) module performs guided refinement of context tokens, which encode context-specific information over the entire temporal sequence, thereby enabling more effective final-stage feature integration within individual contexts. For context i, the updated context token \tilde{f}_i^{rels} from the CCF module retain their inherent contextual information while simultaneously integrating crosscontextual knowledge, which is further propagated during intra-context refinement. \tilde{f}_i^{rels} is then prepended to the contextual feature sequences output from the ICF module. These sequences are then processed by a feed-forward network (FFN) with residual connections and normalization, refined contextual sequences $\overline{\overline{F}}_i = [\overline{f}_i^{cls}, \overline{f}_i^{t-N+1}, ..., \overline{f}_i^t].$

Finally, a guided intra-context attention (GI-Attn) mechanism aggregates temporal dependencies within each context to further refine the corresponding context token. Notably, unlike MI-Attn, which performs interactions over the entire contextual sequence, GI-Attn restricts its operation to refining the context token. GI-Attn consists of multiple attention heads. For attention head h, the query is generated by linearly projecting the context token $\overline{f}_i^{\, cls}$, whereas the key and value are obtained from the contextual sequence:

$$\overline{Q}_h = \overline{f}_i^{cls} \cdot \overline{W}_{i,h}^Q, \quad \overline{K}_h = \overline{F}_i \cdot \overline{W}_{i,h}^K, \quad \overline{V}_h = \overline{F}_i \cdot \overline{W}_{i,h}^V$$
 (7)

The guided intra-context attention is computed as:

$$\alpha_h^{\text{GI-Attn}} = \text{Softmax}\left(\frac{\overline{Q}_h \cdot \overline{K}_h^T}{\sqrt{d}}\right)$$
 (8)

Where $\alpha_h^{\text{GI-Attn}} \in \mathbb{R}^{1 \times (N+1)}$ denotes the guided intra-context attention matrix that encodes the attention weights between the context token and the contextual sequence.

The context token is further refined by multiplying $\, \alpha_{\scriptscriptstyle h}^{\, {
m GI-Attn}} \,$ with $\, \overline{V_{\scriptscriptstyle h}} \,$.

$$\hat{f}_{ih}^{cls} = \alpha_h^{\text{GI-Attn}} \cdot \overline{V}_h \tag{9}$$

The refined context token \hat{f}_i^{cls} is obtained by concatenating the outputs of all attention heads, followed by a linear projection.

3.6 Cross-Context Refinement

The cross-context refinement (CCR) module consolidates directed cross-context interactions and further refines the global CLS token, which encodes both multi-frame and multi-contextual information, serving as the final-stage multi-context fusion. Specifically, the global CLS token $\tilde{f}_{\rm g}^{\rm rcls}$ generated by the CCF module is concatenated with the

updated context tokens \hat{f}_P^{cls} , \hat{f}_L^{cls} , \hat{f}_V^{cls} , \hat{f}_E^{cls} from the ICR module to form \hat{F}_C , which is passed into the guided crosscontext attention (GC-Attn). Notably, in contrast to MC-Attn, GC-Attn adopts a directed cross-context fusion mechanism, where interactions are restricted to a unidirectional exchange between the global CLS token and the context tokens \hat{F}_C . The architecture of GC-Attn is shown in Fig. 3. GC-Attn consists of multiple attention heads. For the attention head l, the global CLS token is used to generate the query, while the key and value are derived from \hat{F}_C :

$$\hat{Q}_{l} = \tilde{f}_{\sigma}^{\prime cls} \cdot \hat{W}_{l}^{\mathcal{Q}}, \quad \hat{K}_{l} = \hat{F}_{C} \cdot \hat{W}_{l}^{K}, \quad \hat{V}_{l} = \hat{F}_{C} \cdot \hat{W}_{l}^{V}$$
(10)

The guided cross-context attention is computed as:

$$\alpha_l^{\text{GC-Attn}} = \text{Softmax}\left(\frac{\hat{Q}_l \cdot \hat{K}_l^T}{\sqrt{d}}\right)$$
 (11)

Where $\alpha_l^{\text{GC-Attn}} \in \mathbb{R}^{1 \times 5}$ denotes the guided cross-context attention matrix that encodes the attention weights between the global CLS token and all context tokens \hat{F}_C .

Finally, the global CLS token is further refined by multiplying $\alpha_l^{\text{GC-Attn}}$ with $\hat{V_l}$, achieving deeper integration of multi-context information:

$$\tilde{f}_{g,l}^{\textit{mcls}} = \alpha_l^{\text{GC-Attn}} \cdot \hat{V}_l \tag{12}$$

The refined global CLS token $\tilde{f}_g^{\textit{mcls}}$, formed via concatenation of the outputs from all attention heads and a subsequent linear projection, is subsequently processed by a multi-layer perceptron (MLP) to produce the pedestrian intention.

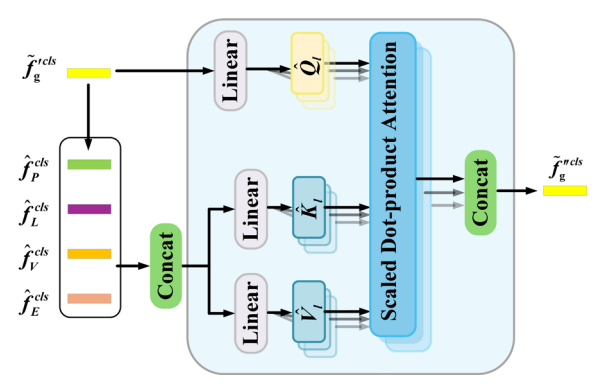


Fig. 3 The architecture of the guided cross-context attention

4. Experiments

4.1 Datasets and Implementation Details

MFT is evaluated on two public benchmarks, JAAD [2] and PIE [3]. JAAD dataset contains 346 HD videos from North America and Eastern Europe. We use its two annotation variants, JAAD_{beh} and JAAD_{all} (the latter includes 2,100 additional non-crossing pedestrians). Following [5], the dataset is split into 177, 117, and 29 videos for training, testing, and validation. From the annotated sequences, 16-frame clips

Table 1. Quantitative results on JAAD dataset

Models	$\mathbf{JAAD_{beh}}$						JAAD _{all}					
Widels	Acc	AUC	F1	Precision	Recall	Acc	AUC	F1	Precision	Recall		
IntFormer [15]	0.59	0.54	0.69	-	-	0.86	0.78	0.62	-	-		
PCPA [5]	0.56	0.54	0.63	0.66	0.60	0.77	0.79	0.56	0.42	0.83		
Global PCPA [4]	0.62	0.54	0.74	0.65	0.85	0.83	0.82	0.63	0.51	0.81		
MMH-PAP [16]	-	-	-	-	-	0.84	0.80	0.62	0.54	-		
TrouSPI-Net [17]	0.64	0.56	0.76	0.66	0.91	0.85	0.73	0.56	0.57	0.55		
ST CrossingPose [18]	0.63	0.56	0.74	0.66	0.83	-	-	-	-	-		
V-PedCross [10]	0.61	0.50	0.75	<u>0.71</u>	0.80	0.82	0.74	0.64	0.58	0.63		
RU-LSTM [20]	0.69	0.62	<u>0.78</u>	-	-	0.86	0.78	0.62	-	-		
STFF-MANet [21]	0.66	0.58	0.77	0.67	0.89	0.89	0.80	0.67	<u>0.68</u>	0.67		
MTMGN [22]	<u>0.70</u>	<u>0.70</u>	0.83	0.79	0.87	0.89	0.89	0.73	0.66	0.89		
Dual-STGAT [23]	-	-	-	-	-	0.92	0.92	0.73	0.86	0.63		
LSOP-Net [24]	0.65	0.54	<u>0.78</u>	0.65	0.98	0.85	0.75	0.58	0.56	0.61		
MFT	0.73	<u>0.70</u>	<u>0.80</u>	<u>0.75</u>	0.86	0.93	<u>0.97</u>	0.83	<u>0.72</u>	0.99		

Table 2. Quantitative results on PIE dataset

Models	PIE								
Models	Acc	AUC	F1	Precision	Recall				
IntFormer [15]	0.89	0.92	0.81	-	-				
PCPA [5]	0.87	0.85	0.78	0.76	0.81				
Global PCPA [4]	0.89	0.86	0.80	0.79	0.81				
MMH-PAP [16]	0.89	<u>0.88</u>	0.81	0.77	-				
TrouSPI-Net [17]	0.88	0.88	0.80	0.73	0.89				
V-PedCross [10]	0.89	0.88	0.67	0.74	0.84				
RU-LSTM [20]	0.87	0.84	0.77	-	-				
STFF-MANet [21]	0.89	0.88	0.82	0.79	0.85				
MTMGN [22]	0.90	0.87	0.92	0.95	0.90				
PFRN [19]	0.90	0.85	0.77	0.81	0.74				
Dual-STGAT [23]	0.86	0.87	0.91	0.92	0.90				
LSOP-Net [24]	0.89	0.87	0.81	0.80	0.82				
MFT	0.90	0.94	0.83	<u>0.83</u>	0.82				

are sampled with 80% overlap. PIE dataset consists of 6 hours of HD video recorded in Toronto with frame-level annotations for 1,842 pedestrians. Following [5], we use set01, set02, and set06 for training, set04 and set05 for validation, and set03 for testing.

The number of attention heads is set to 4 for all multi-head attention mechanisms. Both the embedding space and the Transformer hidden dimension are configured to 128. A dropout rate of 0.2 is applied in the MLP. The batch size is set to 2, and the model is trained for a total of 60 epochs. We employ binary cross-entropy loss and optimize the model using Adam with a learning rate of 5×10^{-7} for JAAD dataset and 2×10^{-5} for PIE dataset. To mitigate class imbalance, we incorporate class weights proportional to the positive–negative sample ratio.

4.2 Quantitative Results

We compare MFT with several state-of-the-art (SOTA) methods. The results on JAAD and PIE datasets are shown in Table 1 and 2, respectively. Green, blue and orange indicate the best, second-best and third-best results, respectively. We evaluate performance with five commonly used metrics: accuracy (Acc), area under the curve (AUC), F1 score, precision, and recall, consistent with the benchmark settings [5].

On the JAAD_{beh} dataset, MFT attains the highest accuracy of 73%, outperforming MTMGN [22] and RU-LSTM [20] by

3% and 4%, respectively. MFT achieves the highest AUC score of 70%, which is comparable to MTMGN [22] and outperforms the third-best method, RU-LSTM [20], by 8%. In terms of F1 score and precision, MFT ranks second with 80% and 75%, respectively. Although these results are 3% and 4% lower than those of the best-performing method, MTMGN [22], they still surpass the third-best methods, outperforming RU-LSTM [20] and LSOP-Net [24] by 2% in F1 score and V-PedCross [10] by 4% in precision. The recall performance is relatively modest, reaching 86%, which lags significantly behind LSOP-Net [24].

On the JAAD_{all} dataset, MFT achieves the highest accuracy of 93%, surpassing Dual-STGAT [23] by 1% and both STFF-MANet [21] and MTMGN [22] by 4%. MFT also demonstrates strong performance in AUC, reaching 97%, which is 5% higher than Dual-STGAT [23] and 8% higher than MTMGN [22]. MFT achieves an F1 score of 83%, outperforming the second-best methods, MTMGN [22] and Dual-STGAT [23], by 10%. MFT also achieves the best performance in recall, reaching 99%. MFT ranks third in precision, falling 14% behind the top-performing method, Dual-STGAT [23].

On the PIE dataset, MFT demonstrates strong competitiveness, achieving an accuracy of 90% and sharing the top position with MTMGN [22] and PFRN [19]. MFT also achieves the best AUC on the PIE dataset, reaching 94%, which is 2% higher than the second-best method, IntFormer [15]. MFT ranks third in both F1 score and precision, with values of 83% and 83%, respectively. Its recall performance is relatively weaker, falling 8% behind the top-performing methods, MTMGN [22] and Dual-STGAT [23].

The quantitative results demonstrate that the proposed MFT network, benefiting from compact and explicitly semantic inputs beyond raw data together with rich and diverse contextual information, effectively captures complementary signals from pedestrians, vehicles, and the traffic environment. Its robust progressive fusion strategy further facilitates multi-stage integration of intra- and cross-context information through dedicated attention mechanisms, thereby improving both the efficiency and effectiveness of feature extraction and fusion. Furthermore, the introduction of a compact global CLS token enhances the network's capacity to encode global semantics and contextual cues, thereby providing comprehensive global information that

leads to superior predictive performance and outperforms SOTA methods.

4.3 Ablation Studies

To assess the effectiveness of the network architecture and contribution of input context, we design and evaluate several architectural variants as follows: (1) MFT-v1: The environmental context E is removed. (2) MFT-v2: The pedestrian behavior context P is removed. (3) MFT-v3: Both the pedestrian behavior context P and environmental context E are removed. (4) MFT-v4: The GC-Attn of CCR module is substituted with a simple pooling operation over all the context tokens. (5) MFT-v5: The GC-Attn of CCR module is substituted with modality attention proposed in Global PCPA [4]. The results are shown in Table 3 and Table 4.

Compared with MFT, MFT-v1 and MFT-v2 show accuracy drops of 4% and 5% on JAAD $_{beh}$ dataset, 5% and 3% on JAAD $_{all}$ dataset, and 3% and 2% on PIE dataset, respectively.

Table 3. Ablation studies on JAAD dataset

Variant	JAAD _{beh} /JAAD _{all}										
v arrant	Acc	AUC	F1	Precision	Recall						
MFT-v1	0.69/0.88	<u>0.77</u> /0.94	0.68/0.75	<u>0.93</u> /0.60	0.53/ <u>1.00</u>						
MFT-v2	0.68/0.90	0.69/0.96	0.78/0.78	0.70/0.65	<u>0.87</u> /0.96						
MFT-v3	0.63/0.76	0.47/0.84	0.76/0.53	0.64/0.41	<u>0.93</u> /0.76						
MFT-v4	0.70/0.91	0.73/0.98	<u>0.79</u> /0.79	0.72/0.66	0.87/0.99						
MFT-v5	0.72/0.92	0.70/0.96	0.79/0.81	<u>0.76/0.69</u>	0.82/ <u>0.99</u>						
MFT	0.73/0.93	0.70/ <u>0.97</u>	0.80/0.83	0.75/ <u>0.72</u>	0.86/ <u>0.99</u>						

Table 4. Ablation studies on PIE dataset

Variant			PIE		
variant	Acc	AUC	F1	Precision	Recall
MFT-v1	0.87	0.92	0.79	0.73	0.87
MFT-v2	0.88	0.93	0.80	0.74	0.87
MFT-v3	0.83	0.91	0.75	0.65	0.87
MFT-v4	0.89	0.94	0.81	0.83	0.78
MFT-v5	<u>0.89</u>	0.93	0.81	0.81	0.81
MFT	0.90	0.94	0.83	0.83	0.82

Among all variants, MFT-v3 shows the largest performance drop, with accuracy decreases of 10%, 17% and 7% on the three datasets, respectively. These results indicate that different contexts provide complementary information that enhances the understanding of pedestrian-vehicle interactions. While omitting either context results in a moderate decline in performance, the simultaneous removal of pedestrian behavior and environmental contexts causes a substantial degradation, underscoring the indispensable role of contextual integration in ensuring robust and accurate predictions. In comparison with MFT, MFT-v4 and MFT-v5 show accuracy decreases of 3% and 1% on JAAD $_{beh}$ dataset, 2% and 1% on JAAD $_{all}$ dataset, and 1% and 1% on PIE dataset, respectively. This demonstrates that the proposed guided cross-context attention mechanism is more effective in integrating complementary information from different contexts.

4.4 Qualitative Results

We present qualitative results for several illustrative cases, where the target pedestrian is enclosed within a red rectangular boundary. Ground truth is indicated by GT, with C and NC representing crossing and non-crossing, respectively. The results are shown in Fig. 4, where we also visualize the average attention scores of the GC-Attn in the CCR module, illustrating the attention of the global CLS token to different contexts within the corresponding scenes.

The results show that MFT can reliably predict pedestrian's intentions across the following cases: In case (a), the pedestrian remains stationary at the roadside in front of a crosswalk, exhibiting no body movement but maintaining eye contact with the vehicle. Under these conditions, MFT successfully predicts the intention to cross, with attention weights primarily focused on the environmental context E (74.5%) and the global CLS token capturing early-stage holistic information (13.1%), while a non-negligible portion is allocated to the pedestrian behavior context P (9.4%). This suggests that MFT effectively outcome integrates environmental cues such as crosswalk availability with subtle behavioral indicators, thereby capturing information beyond

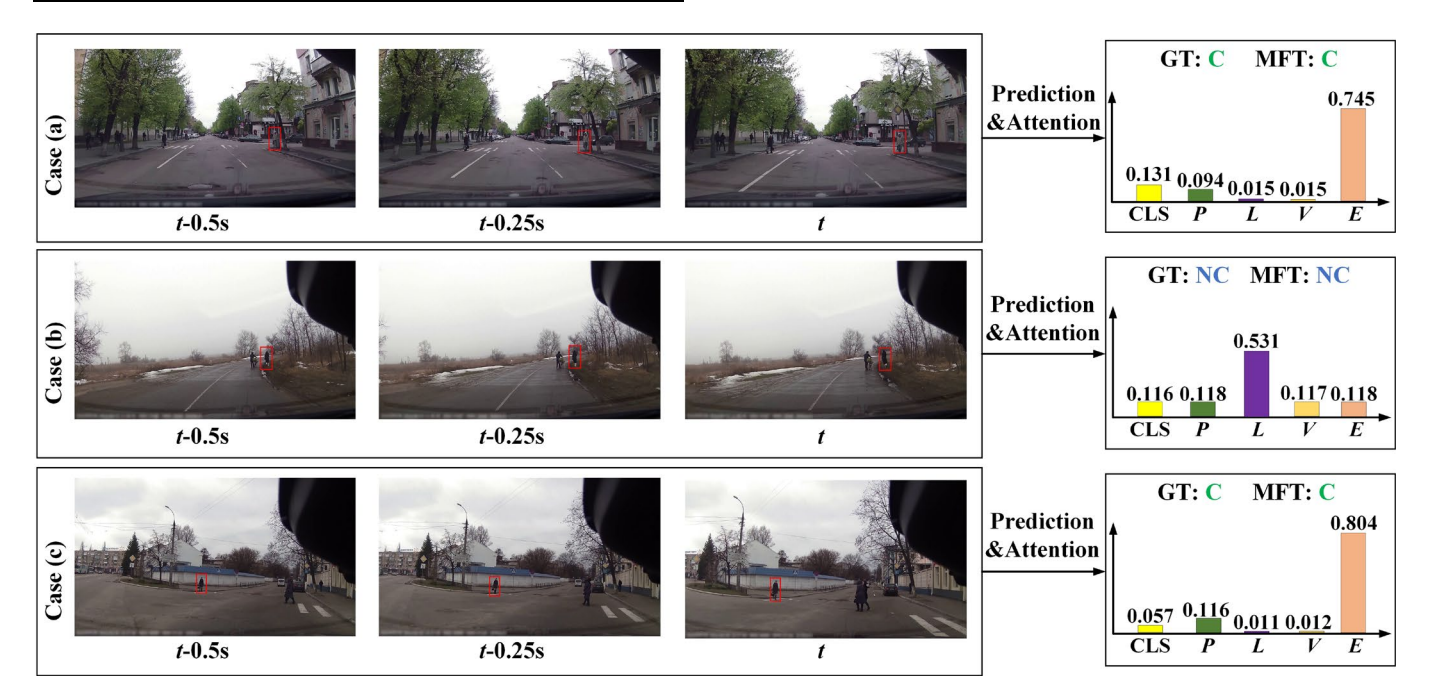


Fig. 4 Qualitative results of MFT network

an immediate motion cues and achieving robust intention prediction in ambiguous scenarios. In case (b), the pedestrian is walking longitudinally along the roadside. MFT accurately predicts a non-crossing intention, with attention primarily focused on the pedestrian localization context L (53.1%), which reflects the pedestrian's consistent lateral position along the road, while the other contexts receive similar levels of attention. In case (c), the scene depicts a woman walking from the roadside toward the crosswalk, accompanied by a pedestrian sign. MFT accurately infers her crossing intention by focusing predominantly on cues from the environmental context E (80.4%), thereby emphasizing the pivotal contribution of traffic infrastructure cues to intention prediction.

4.5 Computational Cost Analysis

We evaluate the real-time performance and computational cost of MFT by comparing it with several baseline methods, including PCPA [5], Global PCPA [4], FUSSI [28], MFFN [29], VMI [26], and MTMGN [27]. For evaluation, we test the model trained on the JAAD dataset as an example. The results are presented in Table 5, where green and blue highlight the best and second-best performance, respectively. MFT achieves the smallest parameter number of 0.95 million, lower than the second-smallest model, FUSSI [28] (1.00 million). Regarding model size, MFT ranks second at 9.40 MB, slightly

larger than FUSSI [28] (8.40 MB) but still smaller than all other methods. In terms of inference time, MFT attains the second-best result of 23.20 ms, slower than VMI [26] (11.03 ms) but notably faster than FUSSI [28] (34.92 ms), which ranks third. The results of the computational cost analysis demonstrate that MFT exhibits competitive model compactness and real-time inference performance.

Table 5. Comparison of computational cost

Models	Size (MB)	Parameters (Million)	Inference Time (ms)
PCPA [5]	118.80	31.17	38.60
Global PCPA [4]	374.20	60.92	70.83
FUSSI [28]	8.40	<u>1.00</u>	34.92
MFFN [29]	-	-	46.20
VMI [26]	19.07	-	11.03
MTMGN [27]	-	-	56.00
MFT	9.40	0.95	23.20

4.6 Attention Map Visualization

We provide visualizations of the multi-head attention maps of MC-Attn mechanism of CCF module and GC-Attn mechanism of CCR module across all test samples to assess the importance of different contexts at different fusion stages. Fig. 5-7 illustrate the multi-head attention maps of MC-Attn mechanism on JAAD $_{\rm beh}$, JAAD $_{\rm all}$, and PIE datasets, respectively.

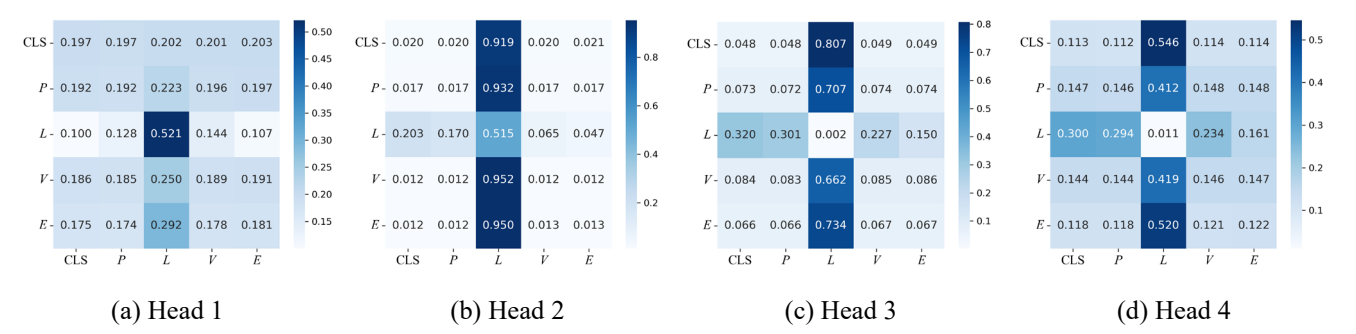


Fig. 5 Visualization of attention maps generated by the MC-Attn mechanism on the JAAD_{beh} dataset

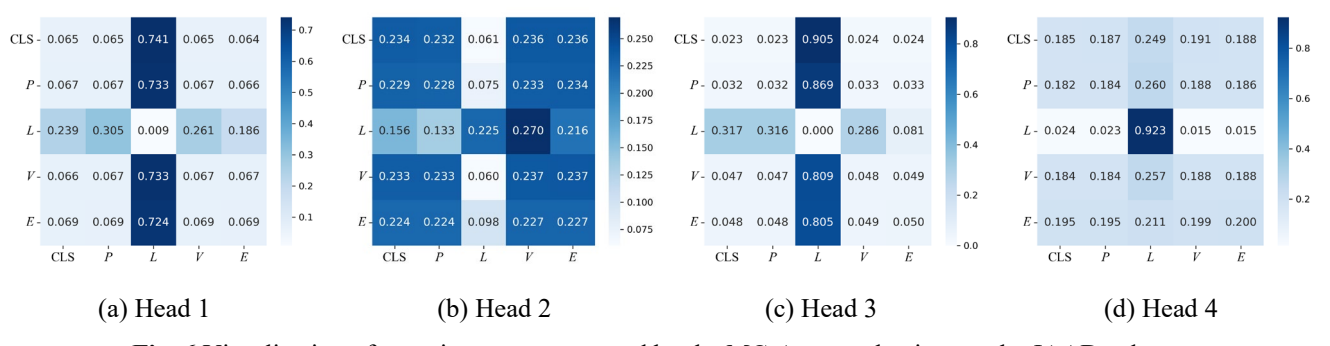


Fig. 6 Visualization of attention maps generated by the MC-Attn mechanism on the JAAD_{all} dataset

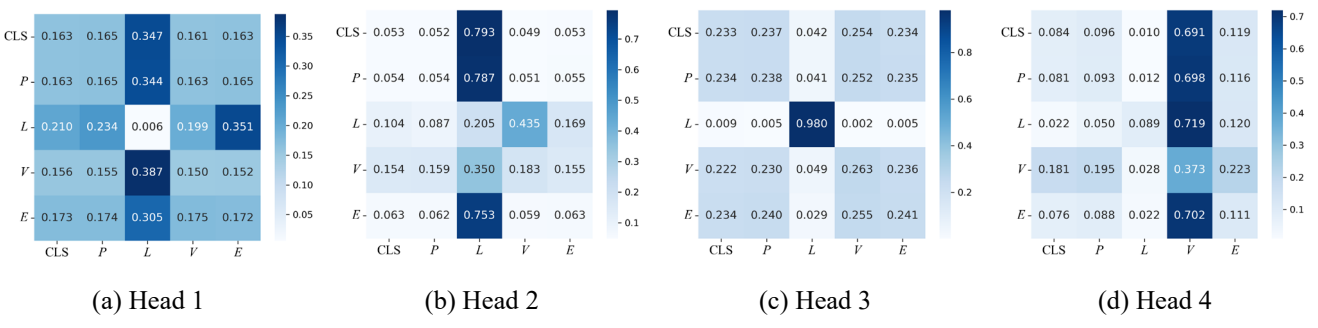


Fig. 7 Visualization of attention maps generated by the MC-Attn mechanism on the PIE dataset

The mutual attention between the global CLS token and the context tokens is clearly depicted, where darker blue indicates stronger attention. In the early stage of fusion, the pedestrian localization context (L), representing the bounding box coordinates of the pedestrian, receives the greatest attention from the global CLS token. Specifically, on the JAAD_{beh} and PIE datasets, three heads exhibit the strongest attention with weights of 91.9%, 80.7%, and 54.6% and 34.7%, 79.3%, and 69.1%, respectively, while on the JAAD_{all} dataset, two heads dominate with weights of 74.1% and 90.5%. In contrast, the attention of other context tokens is more dispersed, with a greater focus on one another while exhibiting weaker selfattention, thereby complementing the information provided by their own context. These observations reveal two key characteristics at the early stage of fusion: (1) The pedestrian localization context L consistently receives dominant attention from the global CLS token, underscoring its crucial role in grounding intention prediction; and (2) Other context tokens interact more with each other than with themselves, indicating complementary information exchange rather than reliance on self-attention.

Figures 8–10 present the multi-head attention maps of the GC-Attn mechanism, illustrating the attention of the global context on all context tokens in the final stage of fusion. It can be observed that the distribution of attention varies across different datasets, and that each head attends to different aspects. On the JAAD_{beh} dataset, three heads primarily attend to the environmental context E with weights of 38.7%, 56.5%, and 41.5%, while one head focuses on the global CLS token, capturing early-stage holistic information, with a weight of 42.1%. On the JAAD_{all} dataset, a comparable pattern emerges: three heads concentrate on the environmental context E with weights of 64.6%, 42.8%, and 40.7%, whereas one head places strong emphasis on the global CLS token with a weight of 84.0%, while the remaining tokens receive a more evenly distributed attention. On the PIE dataset, a different distribution pattern is observed. Only two heads assign attention greater than 40% to specific context tokens, with head 1 attending to the pedestrian behavior context P at 47.0% and head 3 focusing on the vehicle motion context V at 49.3%. The remaining heads exhibit more dispersed attention without a clear dominant focus. Through the visualization of attention maps, the final-stage fusion reveals not only the varying importance of different contexts across datasets but also the distinct roles played by individual heads. These findings demonstrate that the GC-Attn mechanism effectively captures diverse contextual cues, enabling a more comprehensive understanding of pedestrian intention in complex urban environments.

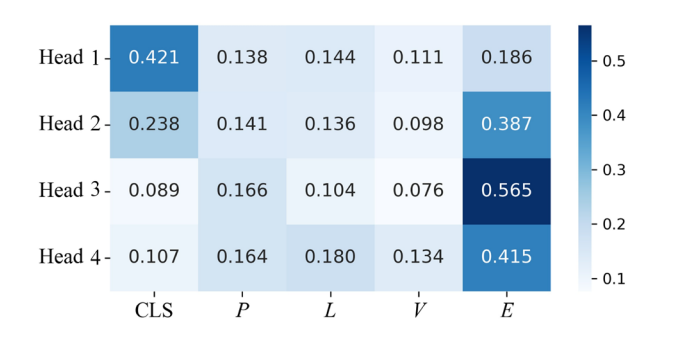


Fig. 8 Visualization of attention maps generated by the GC-Attn mechanism on the JAAD_{beh} dataset

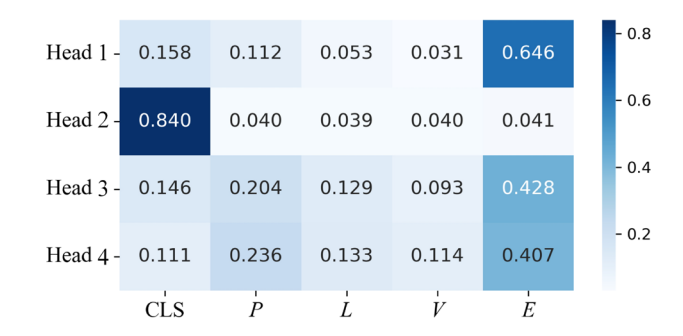


Fig. 9 Visualization of attention maps generated by the GC-Attn mechanism on the JAAD_{all} dataset

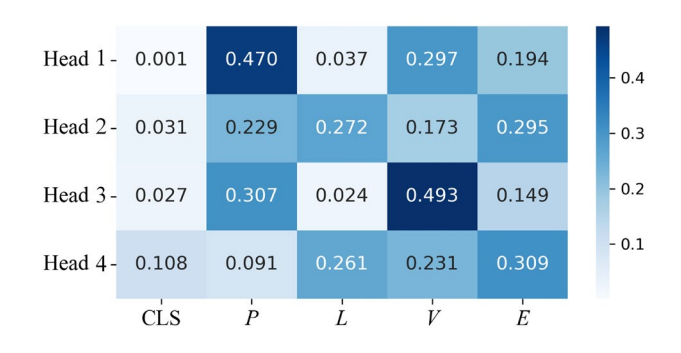


Fig. 10 Visualization of attention maps generated by the GC-Attn mechanism on the PIE dataset

4.7 Effect of Longer Prediction Horizon

While the benchmark setting considers only short prediction horizons of 1–2 seconds [5], we further validate the robustness and effectiveness of the proposed MFT network under extended prediction horizons, thereby assessing its applicability in more challenging scenarios. The time-to-event (TTE) is extended to 2–3 seconds and the resultes on JAAD_{beh}, JAAD_{all}, and PIE datasets are presented in Table 6-8, respectively. It can be observed that a longer TTE leads to decreased model performance, with accuracy dropping from 73% to 68% on JAAD_{beh} dataset, from 93% to 88% on JAAD_{all} dataset, and from 90% to 85% on PIE dataset. This decline arises from the inherent difficulty of making reliable longhorizon predictions, given the unpredictability of urban environments and human behavior.

We also compared MFT with Global PCPA [4] and LSOP-Net [23], two raw-data-based models that exploit implicit cues. The results show that our approach achieves the best performance when the TTE is 2-3 seconds. On the JAAD_{beh} dataset, MFT achieves accuracy improvements of 15% and 2% over Global PCPA [4] and LSOP-Net [23], respectively. On JAAD_{all}, the gains are 9% and 5%, while on the PIE dataset, MFT surpasses them by 7% and 2%. Furthermore, MFT consistently outperforms both baselines across additional evaluation metrics, including AUC, F1 score, and precision, demonstrating its superior robustness and generalization capability. This advantage can be attributed to its use of compact and explicitly semantic contextual attributes. Unlike the implicit and highly entangled nature of raw modality data, attributes provide explicit and interpretable representations, thereby enhancing robustness and enabling more effective generalization over extended prediction horizons.

Table 6. Effect of longer prediction horizon on JAAD_{beh} Dataset

					Time-to-	Event						
Models		1-2s					2-3s					
	Acc	AUC	F1	Precsion	Recall	Acc	AUC	F1	Precsion	Recall		
Global PCPA [4]	0.62	0.54	0.74	0.65	0.85	0.53	0.47	0.65	0.62	0.68		
LSOP-Net [23]	0.67	0.58	0.78	0.67	<u>0.92</u>	0.66	0.56	<u>0.77</u>	0.68	<u>0.90</u>		
MFT	<u>0.73</u>	<u>0.70</u>	<u>0.80</u>	<u>0.75</u>	0.86	<u>0.68</u>	<u>0.61</u>	<u>0.77</u>	<u>0.71</u>	0.83		

Table 7. Effect of longer prediction horizon on JAAD_{all} Dataset

					Time-to-	Event					
Models	1-2s					2-3s					
	Acc	AUC	F1	Precsion	Recall	Acc	AUC	F1	Precsion	Recall	
Global PCPA [4]	0.83	0.82	0.63	0.51	0.81	0.79	0.78	0.57	0.46	0.76	
LSOP-Net [23]	0.84	0.72	0.53	0.54	0.52	0.83	0.72	0.54	0.54	0.54	
MFT	0.93	<u>0.97</u>	0.83	<u>0.72</u>	0.99	0.88	0.94	<u>0.69</u>	0.68	0.69	

Table 8. Effect of longer prediction horizon on PIE Dataset

					Time-to-	Event				
Models			1-2s		2-3s					
	Acc	AUC	F1	Precsion	Recall	Acc	AUC	F1	Precsion	Recall
Global PCPA [4]	0.89	0.86	0.80	0.79	0.81	0.78	0.77	0.65	0.59	0.73
LSOP-Net [23]	0.89	0.86	0.80	0.80	0.80	0.83	0.78	0.68	0.69	0.68
MFT	<u>0.90</u>	<u>0.94</u>	<u>0.83</u>	<u>0.83</u>	0.82	<u>0.85</u>	0.82	<u>0.74</u>	<u>0.72</u>	<u>0.76</u>

5. Conclusion

In this paper, we propose a novel multi-context fusion Transformer (MFT) for pedestrian crossing intention prediction in urban environments. MFT integrates diverse numerical contextual attributes with explicit semantics across four critical dimensions: pedestrian behaviors, environmental conditions, pedestrian localization, and vehicle motion dynamics. To effectively exploit these complementary contexts, MFT adopts a progressive fusion strategy that gradually fuses intra- and inter-context features across multiple stages. Specifically, in the early stage of fusion, mutual intra- and cross-context attentions capture intracontext dependencies and integrate information across contexts, with context tokens and a global CLS token serving as compact context-specific and global representations. In the final stage of fusion, guided intra- and cross-context attentions further refine these representations through directed interactions, yielding deeper and more efficient multi-context integration. Experimental results demonstrate that MFT achieves superior performance compared to the state-of-the-art methods. Moreover, attention visualization enables a deeper assessment of the relative importance of different contexts and enhances the interpretability of MFT. Future research will primarily focus on model lightweighting and practical deployment, with particular attention to reducing computational overhead, optimizing efficiency, and validating the applicability of the proposed network in real vehicle environments.

References

- [1] Yang, B., Yan, S., Wang, Z., et al.: Prediction based trajectory planning for safe interactions between autonomous vehicles and moving pedestrians in shared spaces. IEEE Trans. Intell. Transp. Syst. 24(10), 10513–10524 (2023)
- [2] Rasouli, A., Kotseruba, I., Tsotsos, J.K.: Are they going to cross? A benchmark dataset and baseline for pedestrian crosswalk behavior. Proc. IEEE Int. Conf. Computer Vision Workshops (ICCVW), 206–213 (2017)
- [3] Rasouli, A., Kotseruba, I., Kunic, T., et al.: PIE: A large-scale dataset and models for pedestrian intention estimation and trajectory prediction. Proc. IEEE/CVF Int. Conf. Computer Vision (ICCV), 6262–6271 (2019)
- [4] Yang, D., Zhang, H., Yurtsever, E., et al.: Predicting pedestrian crossing intention with feature fusion and spatio-temporal attention. IEEE Trans. Intell. Veh. 7(2), 221–230 (2022)
- [5] Kotseruba, I., Rasouli, A., Tsotsos, J.K.: Benchmark for evaluating pedestrian action prediction. Proc. IEEE/CVF Winter Conf. Applications of Computer Vision (WACV), 1258–1268 (2021) [6] Rasouli, A. Kotseruba, I. Tsotsos, J.K.: Pedestrian action
- [6] Rasouli, A., Kotseruba, I., Tsotsos, J.K.: Pedestrian action anticipation using contextual feature fusion in stacked RNNs. arXiv preprint, arXiv:2005.06582 (2020)
- [7] Saleh, K., Hossny, M., Nahavandi, S.: Intent prediction of pedestrians via motion trajectories using stacked recurrent neural networks. IEEE Trans. Intell. Veh. 3(4), 414–424 (2018)
- [8] Achaji, L., Moreau, J., Fouqueray, T., et al.: Is attention to bounding boxes all you need for pedestrian action prediction? Proc. IEEE Intell. Veh. Symp. (IV), 895–902 (2022)
- [9] Fang, Z., López, A.M.: Is the pedestrian going to cross? Answering by 2D pose estimation. Proc. IEEE Intell. Veh. Symp.

- (IV), 1271-1276 (2018)
- [10] Bai, J., Fang, X., Fang, J., et al.: Deep virtual-to-real distillation for pedestrian crossing prediction. Proc. IEEE Int. Conf. Intell. Transp. Syst. (ITSC), 1586–1592 (2022)
- [11] Abbasi, J.A., Imran, N.M., Das, L.C., et al.: WatchPed: Pedestrian crossing intention prediction using embedded sensors of smartwatch. Proc. IEEE/RSJ Int. Conf. Intell. Robots and Systems (IROS), 9574–9581 (2023)
- [12] Zhou, Y., Tan, G., Zhong, R., et al.: PIT: Progressive interaction transformer for pedestrian crossing intention prediction. IEEE Trans. Intell. Transp. Syst. 24(12), 14213–14225 (2023)
- [13] Chen, X., Zhang, S., Li, J., et al.: Pedestrian crossing intention prediction based on cross-modal Transformer and uncertainty-aware multi-task learning for autonomous driving. IEEE Trans. Intell. Transp. Syst. 25(9), 12538–12549 (2024)
- [14] Osman, N., Camporese, G., Ballan, L.: Multi-modal transformer with language modality distillation for early pedestrian action anticipation. Comput. Vis. Image Underst. 249, 104144 (2024) [15] Lorenzo, J., Parra, I., Sotelo, M.A.: Intformer: Predicting pedestrian intention with the aid of the Transformer architecture. arXiv preprint, arXiv:2105.08647 (2021)
- [16] Rasouli, A., Yau, T., Rohani, M., et al.: Multi-modal hybrid architecture for pedestrian action prediction. Proc. IEEE Intell. Veh. Symp. (IV), 91–97 (2022)
- [17] Gesnouin, J., Pechberti, S., Stanciulcscu, B., et al.: TrouSPI-Net: Spatio-temporal attention on parallel atrous convolutions and U-GRUs for skeletal pedestrian crossing prediction. Proc. IEEE Int. Conf. Automatic Face and Gesture Recognition (2021)
- [18] Zhang, X., Angeloudis, P., Demiris, Y.: ST CrossingPose: A spatial-temporal graph convolutional network for skeleton-based pedestrian crossing intention prediction. IEEE Trans. Intell. Transp. Syst. 23, 20773–20782 (2022)
- [19] Lv, N., Huang, Y., Zhang, H., et al.: Pedestrian crossing prediction with pathwise feature fusion and stacked gate recurrent unit. IEEE Sensors Lett. 8(2), 1–4 (2024)
- [20] Osman, N., Cancelli, E., Camporese, G., et al.: Early pedestrian intent prediction via features estimation. Proc. IEEE Int. Conf. Image Processing (ICIP), 3446–3450 (2022)
- [21] Zhang, X., Wang, X., Zhang, W., et al.: Multi-attention network for pedestrian intention prediction based on spatio-temporal feature fusion. Proc. Inst. Mech. Eng. D: J. Automobile Eng. 238, 4202–4215 (2024)
- [22] Chen, X., Zhang, S., Li, J., et al.: Explainable pedestrian crossing intention prediction based on multi-task mutual guidance network. IEEE Trans. Intell. Veh. (2024)
- [23] Lian, J., Luo, Y., Wang, X., et al.: Dual-STGAT: Dual spatiotemporal graph attention networks with feature fusion for pedestrian crossing intention prediction. IEEE Trans. Intell. Transp. Syst. (2025) [24] Liu, H., Liu, C., Chang, F., et al.: Long–Short Observationdriven Prediction Network for pedestrian crossing intention prediction with momentary observation. Neurocomputing 614, 128824 (2025)
- [25] Lv, N., Huang, Y., Zhang, H., et al.: Pedestrian crossing prediction with pathwise feature fusion and stacked gate recurrent unit. IEEE Sensors Lett. 8(2), 1–4 (2024)
- [26] Sharma, N., Dhiman, C., Indu, S.: Visual-motion-interaction-guided pedestrian intention prediction framework. IEEE Sensors J. 23(22), 27540–27548 (2023)
- [27] Yang, B., Fan, Z., Hu, H., et al.: Explainable pedestrian crossing intention prediction based on multi-task mutual guidance network. IEEE Trans. Intell. Veh. (2024)
- [28] Piccoli, F., Balakrishnan, R., Perez, M.J., et al.: FUSSI-Net: Fusion of spatio-temporal skeletons for intention prediction network. Proc. Asilomar Conf. Signals, Systems, and Computers (2020)
- [29] Ni, R., Yang, B., Wei, Z., et al.: Pedestrians crossing intention anticipation based on dual-channel action recognition and hierarchical environmental context. IET Intell. Transp. Syst. 17(2), 255–269 (2023)

- [30] Zhao, S., Li, H., Ke, Q., Liu, L., Zhang, R.: Action-ViT: Pedestrian intent prediction in traffic scenes. IEEE Signal Process. Lett. 29, 324–328 (2021)
- [31] Lorenzo, J., Alonso, I.P., Izquierdo, R., et al.: CAPformer: Pedestrian crossing action prediction using Transformer. Sensors 21(17), 5694 (2021)